PAPER • OPEN ACCESS

Graphene exfoliation in cyrene for the sustainable production of microsupercapacitors

To cite this article: Pedro Moreira *et al* 2025 *J. Phys. Energy* **7** 035005

Journal of Physics: Energy

PAPER

Graphene exfoliation in cyrene for the sustainable production of microsupercapacitors

Pedro Moreira[1], **David Carvalho**[1], **Rodrigo Abreu**[1], **Maria D Alba**[2], **Joaquín Ramírez-Rico**[2,3], **Elvira Fortunato**[1], **Rodrigo Martins**[1], **Joana Vaz Pinto**[1], **Emanuel Carlos**[1,*] and **João Coelho**[1,2,3,*]

[1] CENIMAT|i3N, Department of Materials Science, Faculty of Science and Technology, Universidade NOVA de Lisboa and CEMOP/UNINOVA, Campus da Caparica, Caparica, 2829-516, Portugal
[2] Instituto de Ciencia de Materiales de Sevilla, CSIC—Universidad de Sevilla, Avda. Américo Vespucio 49, 41092 Seville, Spain
[3] Dpto. Física de La Materia Condensada, Universidad de Sevilla, Avda. Reina Mercedes SN, 41012 Seville, Spain
[*] Authors to whom any correspondence should be addressed.

E-mail: e.carlos@fct.unl.pt and jmesquita@us.es

Keywords: graphene, cyrene, energy storage, flexible electronics, sustainable fabrication

Supplementary material for this article is available online

OPEN ACCESS

RECEIVED
4 February 2025

REVISED
14 March 2025

ACCEPTED FOR PUBLICATION
8 April 2025

PUBLISHED
22 April 2025

Abstract

Graphene and its composites have attracted much attention for applications in energy storage systems. However, the toxic solvents required for the exfoliation process have hampered the exploitation of its properties. In this work, graphene dispersions are obtained via liquid phase exfoliation (LPE) of graphite in cyrene, an environmentally friendly solvent with solubility parameters like those of N-methyl-2-pirrolidone. The obtained dispersions with a concentration of 0.2 mg ml^{-1} comprised multilayered graphene sheets with lateral sizes in the hundreds of nanometers, as confirmed by scanning electron microscopy, transmission electron microscopy, and Raman spectroscopy. Mixing the obtained dispersions with ethanol made it possible to collect the graphene, which was redispersed in 2-Propanol. This active material was used to fabricate supercapacitor electrodes using a scalable spray deposition method on carbon nanotube (CNT) current collectors with the aid of vinyl masks. The device, tested with a PVA/LiCl gel electrolyte, achieved a specific capacitance of 3.4 mF cm^{-2} (0.015 mA cm^{-2}). In addition, the devices show excellent cycling stability (>10 000 cycles at 0.5 mA cm^{-2}) and good mechanical properties, losing less than 10% of initial capacitance after 1000 bending cycles. This work demonstrates the adaptability of liquid-phase exfoliation to produce graphene sustainably, providing the proof-of-concept for further 2D materials processing and green microsupercapacitor (MSC) fabrication.

1. Introduction

Since its discovery, graphene, a single layer of carbon atoms arranged in a two-dimensional (2D) honeycomb lattice, has attracted immense scientific and technological interest. Its extraordinary properties, including high electrical conductivity, mechanical strength, thermal conductivity, and a large specific surface area, have positioned it as a promising material for a wide range of applications, namely microsupercapacitors (MSCs) [1–5]. Although initially isolated by micromechanical exfoliation, the development of graphene inks compatible with traditional deposition methods has led to the design of a variety of MSCs. Graphene based MSCs have been already fabricated by spray coating [6–8], inkjet printing [9–11], screen-printing [12–14], among others. Liquid-phase exfoliation (LPE) has emerged as a cost-effective and scalable approach for producing graphene inks [15–17]. LPE is a process where bulk graphite is dispersed in a solvent and subjected to ultrasonic energy or shear forces to separate the layers into single or few-layer graphene sheets [18, 19]. The choice of solvent is critical in this process as it influences the exfoliation efficiency and the quality of the resulting graphene. Traditionally, solvents like N-methyl-2-pyrrolidone (NMP), dimethylformamide have been used for LPE due to their ability to match the surface energy of graphene,

facilitating the exfoliation process [20–22]. However, these solvents are toxic, volatile, and pose significant environmental hazards, leading to a growing demand for greener alternatives. This has spurred interest in sustainable solvents, with cyrene (dihydrolevoglucosenone) emerging as a notable candidate due to its green credentials and effectiveness. Cyrene is a bio-based solvent derived from renewable cellulose. It has gained attention as a sustainable alternative due to its low toxicity, biodegradability, and excellent solvating properties [23–26]. Several studies have demonstrated the effectiveness of cyrene for graphene exfoliation as its solubility parameters (δ_D; δ_P; δ_H) of (18.7 $MPa^{1/2}$; 10.8 $MPa^{1/2}$; 6.9 $MPa^{1/2}$) are very similar to those of NMP (18.0 $MPa^{1/2}$; 12.3 $MPa^{1/2}$; 7.2 $MPa^{1/2}$) and graphite (18.0 $MPa^{1/2}$; 9.3 $MPa^{1/2}$; 7.7 $MPa^{1/2}$) [20, 27–31]. For instance, Salavagione *et al* compared the exfoliation efficiency of cyrene with NMP and found that cyrene produced a higher concentration of graphene with fewer defects [31]. The study highlighted cyrene's superior ability to stabilize graphene, resulting in a higher-quality product. Other studies explored the scalability of the process, demonstrating that large quantities of high-quality graphene could be produced using cyrene in a scalable and environmentally friendly manner [29, 32]. However, there are still some challenges to consider regarding processing materials in cyrene. Its high viscosity (14.5 cP) and boiling point (227 °C) can present practical challenges during the exfoliation process and subsequent steps like purification and deposition, usually requiring solvent exchange approaches [33, 34]. Nevertheless, cyrene's use in graphene exfoliation is a relatively new area of research and more studies are needed to fully understand its long-term viability and optimize processing techniques.

In this work, we explore the use of cyrene as suitable solvent for the exfoliation of graphene and subsequent solvent exchange process, so it can be used in scalable spray coating methods. As a proof of concept, the obtained dispersions are used to prepare interdigitated MSCs composed of carbon nanotube (CNT) current collectors and graphene as the active material. The presented methodology allows for a greener and sustainable device fabrication.

2. Experimental methods

2.1. Graphene exfoliation and solvent exchange

In a normal procedure, 1.5 g of graphite flakes (Sigma-Aldrich-+ 200 mesh particle size) were mixed with 30 ml of cyrene in centrifuge tubes with the aid of a vortex mixer. The dispersions were then processed in a Fisherbrand (11207) ultrasonic bath (60% power, 37 kHz) for 8 h, followed by centrifugation in a Sorvall ST8 Centrifuge (4500 rpm (RCF = 3260)) for 90 min and collection of the supernatant (top 90% volume). Due to cyrene's high viscosity, the obtained dispersions were further centrifuged in a Sigma 3–18KS (10000 rom (RCF = 9300)) centrifuge for 30 min followed by the collection of supernatant (80%). The concentration of the dispersions was determined by filtering 15 ml on a pre-weighed Whatman alumina Anodisc filter discs (0.02 μm pore size). Then, 10 ml of the obtained dispersions were mixed with 30 ml of ethanol (1:3) and centrifuged in a Sigma 3–18KS (14600 rpm (RCF = 20018)) centrifuge for 45 min to precipitate the graphene. The supernatant was discarded, and 10 ml of 2-Propanol (Sigma-Aldrich) were added to the centrifuge tubes followed by vigorous stirring in a Fisherbrand (F202A0280FI) vortex mixer. This process was conducted 3 times to ensure complete cyrene removal. The obtained clean samples were re-dispersed in 10 ml of 2-Propanol and stored for further processing. All chemicals were used as purchased without further treatment.

2.2. Characterization Techniques

Scanning electron microscopy (SEM) was used to evaluate the morphology of the raw materials and deposited electrodes in a FEI Teneo, under high vacuum at an operating voltage of 5 keV and a working distance of 10.0 mm. A 10 nm platinum coating was deposited on the samples to reduce charge effects. Further morphological characterization was conducted by transmission electron microscopy (TEM) in a FEI Talos S200 operated at 200 keV in bright field configuration. Raman and x-ray photoelectron spectroscopy (XPS) analysis was used to study the structural composition of the prepared samples. Raman measurements on both graphene inks were collected by a LabRAM Horiba Jobin Yvon confocal Raman microscope using an excitation line of 532 nm with a 100x objective lens, a 250 scans collection in the range between 900 and 3000 cm^{-1}. XPS analyzes were performed using a SPECS Phoibos 150 instrument with a non-monochromatic Al Kα x-ray source (15.4 mA, 13 kV). The instrument's binding energy (BE) scale (work function) was calibrated to give a BE of 84.0 eV for the $Au4f_{7/2}$ signal from freshly ion-etched metallic gold (Au). The spectrometer dispersion (energy range) was adjusted to give a BE of 932.62 eV for the Cu $2p_{3/2}$ line of freshly ion-etched metallic copper (Cu). A charge compensation system (neutralizer) was used for all non-conductive samples. The surface of each non-conductive sample was irradiated with an accelerated electron flow at 2.0–5.0 eV to produce a nearly neutral surface charge. Scanning analyzes (range 0–1350 eV) were performed using a step energy of 50 eV. High energy resolution analyzes of the chemical

state (range 20–50 eV) were performed using a step energy of 20 eV. Additionally, a scan (range of 0–1150 eV) was performed with a non-monochromatic Mg K alpha x-ray source (15.4 mA, 13 kV) using a pass energy of 50 eV. All samples have been deposited with gold (Agar sputter coater equipment) so that the data can be corrected (referenced) by loading using the $Au4f_{7/2}$ signal. CasaXPS v.2.3.26PR1.0 software was used to perform curve fitting, after performing a Shirley background correction, and to calculate the atomic concentrations. Curve fitting of Al2s and O1s spectra were performed using a Gaussian–Lorentzian peak shape. For the analysis of C1s spectra, starting fitting parameters like the approach taken for Biesinger were used [35]. These starting fitting parameters include the main peak asymmetry (defined using an asymmetric Lorentzian line shape) and π to π^* shake-up satellite typical of graphite.

2.3. MSC electrode fabrication

For depositing the MSC electrodes, interdigitated patterns with a finger width of 0.8 mm, length of 10 mm and spacing of 0.8 mm were produced by cutting interdigitated electrode (IDE) patterns in a 76 μm adhesive vinyl using a Silhouette Portrait plotter and transferred to polyimide substrates. The IDE were then peeled off from the substrate creating an adhesive stencil that worked as a physical mask during the deposition. The spray coating was conducted with an airbrush over a hot plate ($\sim$ 10 cm) at 85 °C to promote fast solvent evaporation. First, 50 ml of a 0.1 mg ml^{-1} dispersion of Carbon Solutions P3 single wall CNTs (SWCNTs) in 2-Propanol were deposited by spray-coating to create the current collectors. The SWCNTs dispersion formulation can be found elsewhere [36]. The electrode sheet resistance was measured in an Ossila Four-Point Probe system. Then the previously prepared graphene dispersions were sprayed over the fingers in an area of $\sim$1 cm^2. At the end, the vinyl masks were removed leaving the deposited SC behind. The current collectors (0.5 cm $\times$ 0.5 cm) were coated with silver paste and cured for 1 h at 60 °C. An aqueous PVA/LiCl gel was used as a solid electrolyte. Typically, 4 g of PVA were added to 40 ml of distilled water at 90 °C with continuous stirring. After complete solubilization of the PVA, 8.5 mg of LiCl was added to the solution. The mixture was kept under continuous stirring and heating until it became a transparent gel. Prior to electrolyte casting, the MSCs were cured in an Ossila UV Ozone Cleaner for 15 min at room temperature to reduce the hydrophobicity of graphene. The electrolyte was then drop-cast onto the graphene layer. The assembled SCs were allowed to dry overnight at room temperature before the electrochemical testing.

2.4. Electrochemical characterization

The as-prepared MSCs were characterized in a CS310X potentiostat (Corrtest Instruments) by means of cyclic voltammetry (CV) (5–1000 mV s^{-1}), galvanostatic charge discharge (GCD) (0.015–1 mA cm^{-2}) experiments and electrochemical impedance spectroscopy (5 mV, 1 MHz to 10 mHz). The device specific areal capacitance, C, was calculated from charge–discharge curves as follows:

$$C = \frac{I\Delta t}{A\Delta V} \tag{1}$$

where I is the applied current, Δt is the discharge time, A is the SC active area, and $\Delta V = V_2 - V1$ where V_2 is the potential at the beginning of discharge, after the iR potential drop, and V_1 is the potential at the end of discharge. Areal energy (E) and power (P) densities per unit area were calculated as follows:

$$E = \frac{1}{2}\frac{C\Delta V^2}{3600} \tag{2}$$

$$P = \frac{E}{\Delta t} \times 3600 \tag{3}$$

where 3600 is a conversion factor from Ws to Wh. The deformation tests were conducted by acquiring CVs at 10 mV s^{-1} after 10 essays of 100 bending cycles in a total of 1000 bending tests.

3. Results and discussion

3.1. Graphene processing and ink formulation

In this work, commercial graphite flakes were used as the starting material for the exfoliation process and processing of graphene in cyrene (GC). Figure 1(a) shows a SEM micrograph of an unprocessed flake exhibiting the characteristic layered structure of graphite. After sonication, a dark ink is obtained, as shown in figure 1(b), composed of thin graphene sheets with lateral sizes in the order of hundreds of nanometers (figure 1(c)). The concentration of these inks was determined to be $\sim$0.2 mg ml^{-1}, corresponding to an exfoliation yield (%E) of 0.4%.

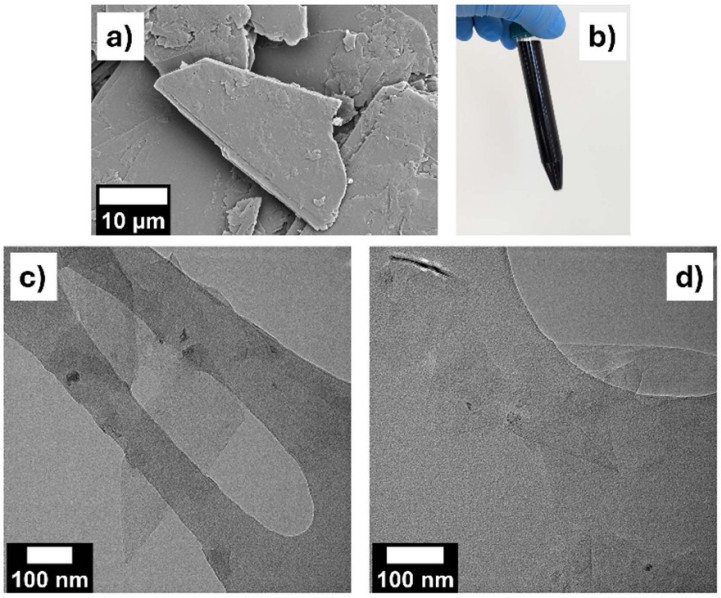

Figure 1. Examples of (a) graphite flakes under SEM; (b) graphene dispersion after sonication; (c) TEM micrographs of the exfoliated graphene in cyrene (GC) and (d) TEM micrographs of graphene after redispersion in 2-Propanol (GP).

In the literature it has been reported concentrations of graphene exfoliated in cyrene as high as 3.70 mg ml^{-1} (%E ∼7.4%) [29] sonicated for 8 h. However, in this specific work, a combination of exfoliation methods (tip sonication and shear mixing) was used to maximize the graphene production yield. Salavagione *et al* obtained a %E of 47% for graphite sonicated in cyrene for 2 h with the aid of a sonic tip [31]. It is evident that the processing conditions of graphene exert a substantial influence on the exfoliation yield. As illustrated in table S1, the graphite starting concentrations and sonication methodologies demonstrate a considerable impact on the production of graphene, even in instances where the same solvents are employed. Additional exfoliation parameters, such as sonication power and duration, and centrifugation speed, also exhibit a substantial effect on the exfoliation yield [37]. Moreover, it cannot be disregarded the structure and flake size of the graphite used. Ng *et al* have recently shown that besides initial concentration, these graphite properties have a significant impact on the exfoliation efficiency of graphene in a wide range of solvents [38]. Additionally, it is also shown that exfoliation efficiency and dispersibility can be analyzed as independent properties. For instance, the mass of graphene per surface area for graphite (particles size ∼150 μm) exfoliated in 2-Propanol was 29 times higher than the values measured for NMP. For a particle size of ∼50 μm, this value rose up to 48. However, this exfoliation efficiency is hindered by the 2-Propanol lower graphene dispersibility, which is also dependent on the graphite properties (graphite morphology, lateral size, defect density, edge defects, *d-spacing*, among others) [38]. As such the reported values for graphene exfoliated in cyrene may in fact vary across different works reported in the literature. For our study, we preferred to use a lower power sonic bath as it causes less damage to the samples and produces larger flakes, although usually at a lower concentration. It was also used longer centrifugation cycles, which probably contributed to further removal of material in suspension. As such, in this work it is shown that it is possible to exfoliate GC and use it for energy storage applications.

As with NMP, the high boiling point of cyrene poses some challenges to its use on a larger scale. Therefore, it is normal to carry out a solvent exchange process. In this work, the obtained dispersions were first mixed with ethanol in a ratio cyrene: ethanol (1:3). The poor dispersibility of these solvents combination greatly facilitates graphene deposition, as a clear transparent supernatant is obtained upon centrifugation. After recovering and cleaning the samples, the graphene was re-dispersed in 2-Propanol (GP—Graphene in Propanol), which has been considered a green solvent, while exhibiting a relatively low boiling-point (82.3 °C). A TEM micrograph of the graphene re-dispersed in 2-Propanol (figure 1(d)) is quite like the original samples processed in cyrene. To investigate if there are structural or chemical changes to the graphene during the solvent exchange process, the samples were examined by means of Raman Spectroscopy and XPS (figure 2).

Figure 2(a) shows the Raman spectra for both GC and GP where the characteristic peaks of graphene can be identified. The D band (∼1350 cm^{-1}) is ascribed to the A_{1g} mode of vibration and it is usually associated with the degree of defects and structural disorder of the carbon matrix. The G band (∼1580 cm^{-1})

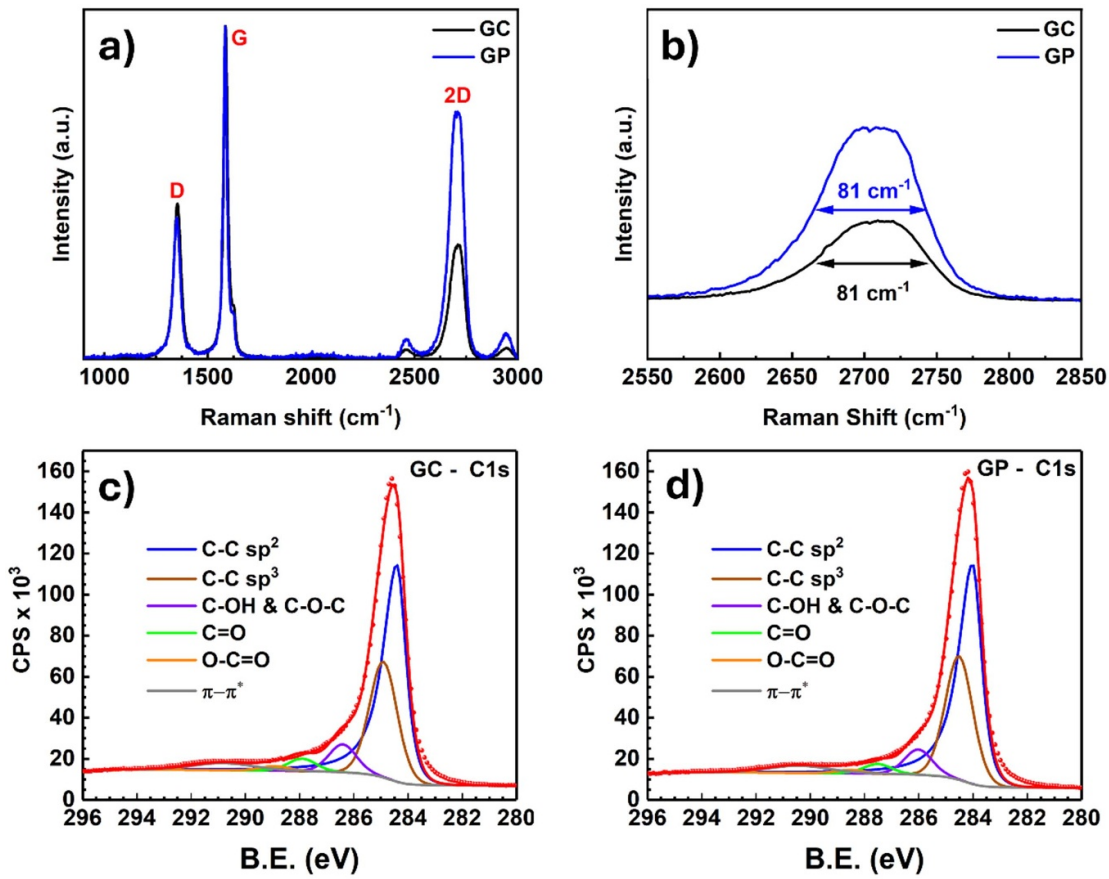

Figure 2. (a) Raman spectra of the graphene samples in cyrene (GC) and 2-Propanol (GP); (b) close-up of the Raman peak of the graphene samples comparing the full width half medium (FWHM) for both samples and (c), (d) XPS spectra for C1s orbitals of GC and GP, respectively.

corresponds to the in-plane $\boldsymbol{E}_{2g}$ vibration mode of C–C bond stretching. Finally, the 2D band (~2700 cm^{-1}), a D-band overtone, results of double resonance between the *K*-points in the Brillouin zone [39, 40]. It has been verified that for monolayer graphene $I_{2D} > I_G$. In our samples, the weaker and symmetrical 2D peak is indicative of a few-layers graphene [41–43]. For the example given in figure 2(a), a more intense 2D peak is observed for GP. In the case of solution processed graphene, extreme care should be taken when analyzing Raman data as random restacking of the flakes and defects can significantly change the spectra [42]. The full width-half medium (FWHM) of 2D peak is also indicative of number of layers in a sample. In this work, the FWHM for GC and GP was measured as ~81 cm^{-1} (figure 2(b)), which may be indicative of the same number of layers for both samples. Nevertheless, no significant changes are observed for either GC or GP spectra. As such, based on previous literature, it is safe to assume that the Raman spectrum corroborates the observations made for the TEM micrographs. Figures 2(c) and (d) show the C1s spectra of both graphene samples exhibiting the characteristic C–C sp^2 signal graphitic carbon at 284.4 eV. The π-π^* transition loss peak is detected at 291.5 eV [44]. Other chemical shifts are detected at 286.4 eV, 287.9 eV and 289.9 eV which are typically assigned to C–OH/C–O–C, C = O and O-C = O functional group respectively [35, 44]. It is common to observe oxygenated species in exfoliated graphene due to residual solvent molecules. In addition, as the measurements were performed in filtered films, it is possible that a larger amount of solvent is trapped in the layers of the filtrate. Moreover, shown by Skaltsas *et al* sonication induces defects and oxygenated species on graphene which contribute to the sp^3 signal [45, 46]. This observation is in good agreement with the D peak observed in the Raman spectra. The fact that the D and G bands are not broad (as observed for graphene oxide and reduced graphene oxide) suggests that the defects present are not basal plane defects but rather edge defects [46]. Finally, the sp^3 signal located at 285.3 eV can also be attributed to the presence of adventitious carbon on the sample. Further XPS analysis confirming the presence of graphene can be found in the provided supplementary information (section S2). The XPS data corroborates the Raman results, showing that no damage or sample deterioration occurred during the solvent exchange process. As such, GP will be tested as supercapacitor electrode active material in the following sections.

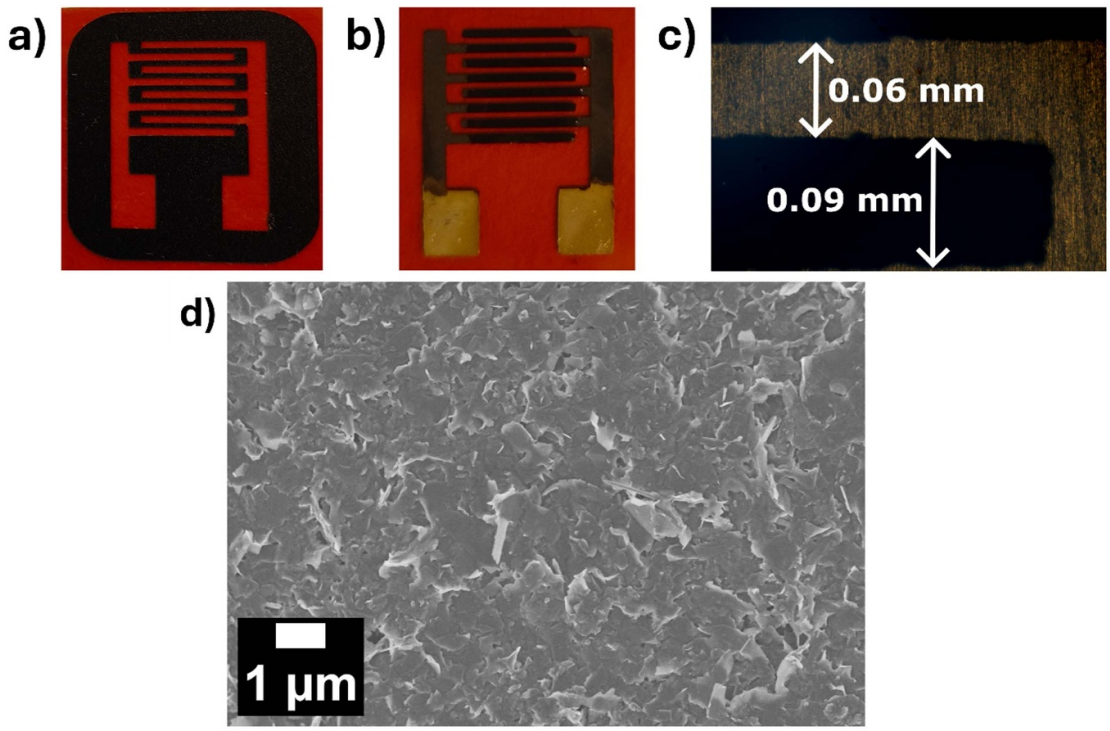

Figure 3. (a) vinyl mask on polyimide substrate; (b) spray-coated MSC; (c) 5x magnification of the interfingers spacing and (d) SEM micrograph of the deposited graphene film.

3.2. Electrode fabrication and characterization

In this work, the MSC electrodes were fabricated by spray coating the GP into a polyimide substrate (Kapton) with the aid of adhesive vinyl masks as shown in figure 3(a). First, a conductive SWCNT layer was spray coated over the whole mask to deposit the current collectors (~20 Ω sq^{-1}). In this work, SWCNTS with 1–3 atomic % carboxylic acid groups were used due to their dispersability in 2-Propanol. Then, 10 ml of the GP dispersions were deposited over the fingers area to achieve a mass loading of ~1 mg cm^{-2}. After painting the silver electrical contact pads, the mask is lifted, a gel electrolyte is applied to the GP coated fingers and a complete device is obtained (figure 3(b)). This device has (2 cm × 2 cm) composed of fingers with ~0.09 mm separated by a 0.06 mm gap (figure 3(c)). The magnification of the sprayed GP (figure 3(d)) shows that it is composed of sheet-like graphene flakes. Regarding dimensions, they seem to be in good agreement with the TEM micrographs (figure 1(d)). Larger graphene flakes could be expected for sonic bath processing cyrene's high viscosity may also contribute towards the stabilization of larger flakes. The full process for the preparation of the masks and MSC fabrication is described in the provided supplementary information (section S3).

The electrochemical and energy storage properties of these GP-based MSC were extensively analyzed through CV and GCD tests. PVA/LiCl was employed as the electrolyte, while the GP and CNT layers served as the MSC active material and current collectors, respectively. These results are shown in figure 4. The CV curves (figure 4(a)) display a quasi-rectangular shape (5–100 mV s^{-1}), typical of carbon-based electric double-layer capacitors, suggesting good electrochemical stability. CV curves up to 1 V s^{-1} are depicted in figure S7(a). These results are further corroborated by the GCD curves presented in figure 4(b), where the nearly ideal symmetric triangular shapes and minimal voltage drop indicates a strong capacitive behavior. By applying equation (1) to the discharge curves, the areal capacitance, C, was calculated for the different currents applied during the GCD tests (figure 4(c)).

A maximum capacitance of 3.34 mF cm^{-2} was measured for a current density of 0.015 mA cm^{-2}. At a higher current density of 0.5 mA cm^{-2}, the GP MSC still demonstrates a C of 1.34 mF cm^{-2} (figure 4(c)). These results are in line with other graphene and carbon based MSC. Shi *et al* reported a C of 4.9 mF cm^{-2} (at 2 mV s^{-1}) for spray coated Graphene/PEDOT: PSS composites [47]. Coelho *et al* prepared laser-induced graphene (LIG)—MSC on paper delivering 4.6 mF cm^{-2} (0.015 mA cm^{-2}). Finally, Mendonza-Sanchez *et al* measured a specific capacitance of 0.543 mF cm^{-2} for ultra-thin electrodes of graphene exfoliated in liquid phase [46]. Similar comments can be made regarding energy and power densities (figure S7(b)). The GP spray coated MSC delivered a maximum of 0.23 μWh cm^{-2} (at 0.45 μW cm^{-2}). It is also important to

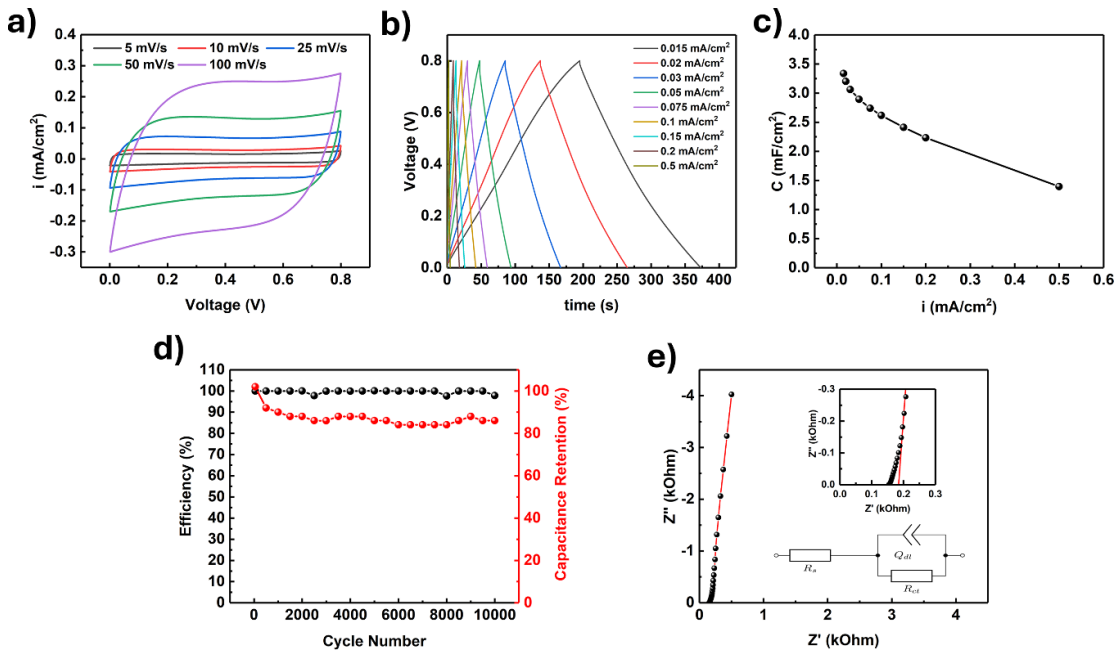

Figure 4. Summary of the electrochemical characterization tests conducted on the GP spray coated supercapacitors: (a) cyclic voltammograms (CV) on the range 5 mV s^{-1}–100 mV s^{-1}; (b) galvanostatic charge discharge curves at current densities ranging from 0.015 mA cm^{-2} to 1 mA cm^{-2} and (c) respective areal capacitance, C; (d) capacitance retention and coulombic efficiency at 0.5 mA cm^{-2} and (e) devices Nyquist plot. For simplicity purposes C will used throughout the text as the symbol for areal capacitance.

mention the fact that there is a capacitance retention of 42% at a current density of 0.5 mA cm^{-2} (figure 4(c)). This capacitance drop is less than ideal, but the GP MSCs were prepared without any conductive additive. PEDOT:PSS is frequently used to lower the sheet resistance of graphene films [29]. However, this polymer can also be used as MSC electrode active material. In fact, graphene and metal oxide particles have been tested as additives for PEDOT:PSS hybrid electrodes [48–50]. To fully study the charge storage capabilities of GP, no conductive materials were added, and thin films were preferred. In terms of cyclability, a 14% capacitance loss is observed after 10 000 cycles (0.5 mA cm^{-2}). However, this process is more evident in the first 1000–2000 cycles, upon which the values of C tend to stabilize (figure 4(d)). There are several factors that affect supercapacitor activity, leading to device degradation and eventual loss of capacitance. Electrolyte decomposition and water evaporation, as well as eventual delamination of active materials and the presence of residual contaminants, are known effects that contribute to capacitance fading in supercapacitors [51, 52]. For the GP-based microsupercapacitors, capacitance degradation is more pronounced in the first cycles, suggesting that it is more likely based on the stabilization of the electrolyte water content and the possible presence of species that contribute to non-reversible reactions. After 2000 cycles, the specific capacitance stabilizes and the loss of performance (<2%) is attributed to the aging mechanisms of the supercapacitor, namely electrolyte degradation and loss of surface area [52]. The Coulombic efficiency (figure 4(d)) remains at 97.86% after 10 000 cycles representing a small capacitance loss upon each charge/discharge cycle. The EIS spectrum (figure 4(e)) is characteristic of porous electrodes exhibiting double layer capacitance with frequency dispersion resulting in deviation from verticality of the capacitive (low frequency) branch, with no appreciable pseudocapacitance. The spectrum was fitted using an element (Z_{pores}) implementing the de Levie model for ideally polarizable porous electrodes incorporating a constant phase element, with an additional capacitor (C_{flat}) in parallel to account for the large external area of the electrodes due to the high aspect ratio of graphene platelets ($\chi^2 = 3\ \ 10^{-5}$) [53–55]. The fit reveals an equivalent series resistor (ESR) of ∼160 Ω which is common for this type of device with painted silver contacts [56]. A fit to the impedance spectra using the simplified Randle's model was also performed, but it resulted in a significantly worse fit ($\chi^2 = 80\ \ 10^{-5}$) and a charge-transfer resistance of $\sim 10^8$ kΩ, confirming that the GP spray-coated MSCs stores charge exclusively through the formation of double layer with no charge-transfer due to faradaic reactions. A more in-depth discussion regarding EIS can be found in supplementary information (section S4).

In relation to applications, in-plane interdigitated MSC on polymeric substrates have been proposed as power sources for wearable technologies and other flexible technologies. Consequently, the MSC must withstand considerable mechanical deformation, such as bending and folding, without compromising the

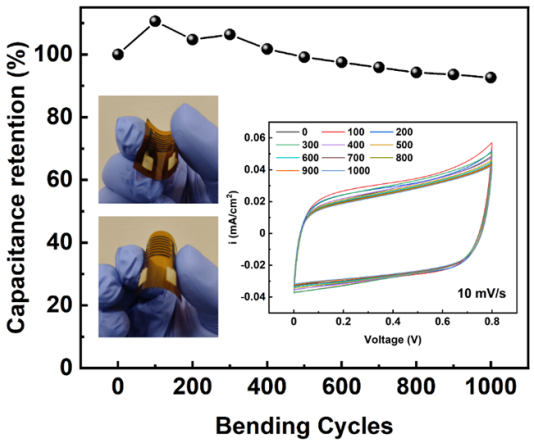

Figure 5. GP MSC capacitance retention as function of 1000 bending cycles. The presented data was acquired from cyclic voltammetry experiments conducted at a scan rate of 10 mV s^{-1}. Bottom left inset:examples of the mechanical deformation applied to the samples and bottom right inset: CVs acquired at each consecutive 100 bending cycles.

overall electrochemical performance. To evaluate the mechanical properties of the GP spray-coated MSC, the prepared samples were subjected to 1000 consecutive cycles of bending, with the specific capacitance measured at every 100th cycle. The results are shown in figure 5.

A capacitance drop of only 8% is observed after 1000 manual bending cycles, suggesting that GP-MSC can be implemented as flexible energy storage devices. However, with adequate encapsulation the MSC may be more stable and retain its capacitance for longer periods of deformation. It is important to point out that a performance uplift (about 10%) can be observed in figure 5. This increase in capacitance has been observed in other flexible devices and is likely to result from an improvement in the electrode/electrolyte interface due to the mechanical deformation, as the electrolyte can penetrate further into the electrode structure and promote the formation of the electrical double layer [57]. It can also be found elsewhere that these devices can easily be arranged in series and parallel to illustrate the scalability and integration capabilities of such systems. As such it is possible to adapt the energy power units to the desired voltages and currents, thus increasing the possible number of applications.

It has been shown in this study that graphene processed in cyrene and then transferred to 2-Propanol (GP) has the potential to be used in spray coated MSC elaboration under low temperatures processing. GP-MSC exhibits figures of merit like other graphene inks but being processed in a much safer and environmentally friendly way being compatible with low-cost flexible substrates such as bio-based polymers and paper [58, 59]. However, due to its porous nature, paper could absorb the inks and lead to device short-circuiting. In this case the proposed electrodes could be used in a sandwich configuration [58]. Better electrochemical performance and higher capacitances can also be obtained by increasing the film thickness and/or using metallic substrates [7, 60, 61]. In these cases, conductive polymers or carbon additives and binders may be required, thus impacting the overall gravimetric capacitance and device flexibility. For instance, Garakani *et al* developed high-power graphene-based supercapacitors operating at a wide range of temperatures [6]. In this study, MSC graphene electrodes were prepared by spray coating onto aluminium current collectors a mixture of graphene, activated carbon and cellulose. In fact, the mixture of graphene with carbon species or dopants (such as nitrogen) has also shown promising results for high performance supercapacitor development [62, 63]. As such, there are a lot of opportunities for GP graphene for further MSC development. In fact, it can be highly relevant for simple, low cost, fast patterning, flexible systems that do not need to adhere to highly controlled environments and sophisticated manufacturing protocols, being poised to occupy a niche in flexible/wearable devices manufacturing and may play a role in fighting the ever-increasing amount of electronic waste (e-waste).

4. Conclusions

This work has demonstrated a sustainable method for the green exfoliation of GC and its subsequent solvent exchange and deposition as an active material for microsupercapacitor electrodes. The solvent exchange process from cyrene to ethanol was found to be very effective without causing any damage or structural changes to the graphene. In addition, the solvent exchange method does not result in any loss or possible contamination compared to graphene isolation by filtration. The use of vinyl masks facilitated the deposition

of the electrodes and can be easily adapted to other designs, further demonstrating the versatility of the proposed methodology.

The spray-coated devices delivered an areal capacitance of 3.34 mF cm^{-2} at a current density of 0.015 mA cm^{-2} and good cyclability and coulombic efficiency after 10 000 cycles (0.05 mA cm^{-2}), performances comparable to other graphene-based microsupercapacitors. Additionaly, the MSC also revealed a considerable mechanical resistance towards mechanical deformation. However, the capacitance retention upon increasing current density should be improved. Nevertheless, the performance of the MSC combined with the exfoliation in cyrene and the versatility of the physical masks used is promising in the context of flexible energy storage devices for IoT applications.

Data availability statement

The data cannot be made publicly available upon publication because they are not available in a format that is sufficiently accessible or reusable by other researchers. The data that support the findings of this study are available upon reasonable request from the authors.

Acknowledgments

The authors acknowledge funding from FCT—Fundação para a Ciência e a Tecnologia, I P, in the scope of the Projects LA/P/0037/2020, UIDP/50025/2020, and UIDB/50025/2020 of the Associate Laboratory Institute of Nanostructures, Nanomodelling and Nanofabrication—i3N. The authors also thank FCT for financial support under the Project 2022.01493.PTDC (GAMBIT). J.C. would like to acknowledge EMERGIA 2021 program (EMC21_00174) from the Consejería de Universidad, Investigación e Innovación, Andalusian Regional Government- Junta de Andalucía. The authors further acknowledge the SUPERIOT project, which has received funding from the Smart Networks and Services Joint Undertaking (SNS JU) under the European Union's Horizon Europe research and innovation programme under Grant Agreement No 101096021, including top-up funding by UK Research and Innovation (UKRI) under the UK government's Horizon Europe funding guarantee. Views and opinions expressed are however those of the authors only and do not necessarily reflect those of the European Union, SNS JU or UKRI. The European Union, SNS JU or UKRI cannot be held responsible for them.

ORCID iDs

Pedro Moreira https://orcid.org/0000-0003-2381-4157
David Carvalho https://orcid.org/0009-0007-1167-9222
Rodrigo Abreu https://orcid.org/0009-0004-2007-2228
Maria D Alba https://orcid.org/0000-0003-0025-3078
Joaquín Ramírez-Rico https://orcid.org/0000-0002-1184-0756
Elvira Fortunato https://orcid.org/0000-0002-4202-7047
Rodrigo Martins https://orcid.org/0000-0002-1997-7669
Joana Vaz Pinto https://orcid.org/0000-0003-0847-7711
Emanuel Carlos https://orcid.org/0000-0002-5956-5757
João Coelho https://orcid.org/0000-0003-4217-3842

References

[1] Zhang F, Yang K, Liu G, Chen Y, Wang M, Li S and Li R 2022 Recent advances on graphene: synthesis, properties and applications *Composites* A **160** 107051
[2] Urade A R, Lahiri I and Suresh K S 2022 Graphene properties, synthesis and applications: a review *JOM* **75** 614–30
[3] Olabi A G, Abdelkareem M A, Wilberforce T and Sayed E T 2021 Application of graphene in energy storage device—A review *Renew. Sustain. Energy Rev.* **135** 110026
[4] Velasco A, Ryu Y K, Boscá A, Ladrón-De-Guevara A, Hunt E, Zuo J, Pedrós J, Calle F and Martinez J 2021 Recent trends in graphene supercapacitors: from large area to microsupercapacitors *Sustain. Energy Fuels* **5** 1235–54
[5] Lakra R *et al* 2021 A mini-review: graphene based composites for supercapacitor application *Inorg. Chem. Commun.* **133** 108929
[6] Garakani M A *et al* 2021 Scalable spray-coated graphene-based electrodes for high-power electrochemical double-layer capacitors operating over a wide range of temperature *Energy Storage Mater.* **34** 1–11
[7] Boulanger N, Skrypnychuk V, Nordenström A, Moreno-Fernández G, Granados-Moreno M, Carriazo D, Mysyk R, Bracciale G, Bondavalli P and Talyzin A V 2021 Spray deposition of supercapacitor electrodes using environmentally friendly aqueous activated graphene and activated carbon dispersions for industrial implementation *ChemElectroChem* **8** 1349–61
[8] Yao F, Li W, K S K S S, Fukuhara C, Badhulika S and Kong C Y 2024 Scalable one-step synthesis of reduced graphene oxide: towards flexible transparent conductive films and active supercapacitor electrodes *Chem. Eng. J.* **488** 150828
[9] Bayoumy A M, Hessein A, Ahmed Belal M, Ezzat M, Ibrahim M A, Osman A and Abd El-Moneim A 2024 Microdrop inkjet printed supercapacitors of graphene/graphene oxide ink for flexible electronics *J. Power Sources* **617** 235145

[10] Peng Q, Tan X, Stempień Z, Xiong W, Venkataraman M and Militky J 2024 Instantaneous reduction of inkjet-printed graphene oxide on PVDF nanofibers for high-performance ultralight flexible supercapacitors *Polym. Test.* **137** 108526
[11] Wen D, Ying G, Liu L, Li Y, Sun C, Hu C, Zhao Y, Ji Z, Zhang J and Wang X 2022 Direct inkjet printing of flexible MXene/graphene composite films for supercapacitor electrodes *J. Alloys Compd.* **900** 163436
[12] Chen H, Chen S, Zhang Y, Ren H, Hu X and Bai Y 2020 Sand-milling fabrication of screen-printable graphene composite inks for high-performance planar micro-supercapacitors *ACS Appl. Mater. Interfaces* **12** 56319–29
[13] Shetty S, Saquib M, Selvakumar M, Firouzi H and Nayak R 2024 Graphene-enhanced manganese dioxide functional ink infused with polyaniline for high-performance screen-printed micro supercapacitor *Mater. Res. Express* **11** 085503
[14] Bellani S, Petroni E, Del Rio Castillo A E, Curreli N, Martín-García B, Oropesa-Nuñez R, Prato M and Bonaccorso F 2019 Scalable production of graphene inks via wet-jet milling exfoliation for screen-printed micro-supercapacitors *Adv. Funct. Mater.* **29** 1807659
[15] Paton K R *et al* 2014 Scalable production of large quantities of defect-free few-layer graphene by shear exfoliation in liquids *Nat. Mater.* **13** 624–30
[16] Morton J A, Kaur A, Khavari M, Tyurnina A V, Priyadarshi A, Eskin D G, Mi J, Porfyrakis K, Prentice P and Tzanakis I 2023 An eco-friendly solution for liquid phase exfoliation of graphite under optimised ultrasonication conditions *Carbon N* Y **204** 434–46
[17] Li Z *et al* 2020 Mechanisms of liquid-phase exfoliation for the production of graphene *ACS Nano* **14** 10976–85
[18] Coleman J N *et al* 2011 Two-dimensional nanosheets produced by liquid exfoliation of layered materials *Science* **331** 568–71
[19] Nicolosi V, Chhowalla M, Kanatzidis M G, Strano M S and Coleman J N 2013 Liquid exfoliation of layered materials *Science* **340** 1226419
[20] Fernandes J, Nemala S S, De Bellis G and Capasso A 2022 Green solvents for the liquid phase exfoliation production of graphene: the promising case of cyrene *Front. Chem.* **10** 878799
[21] Coleman J N 2013 Liquid exfoliation of defect-free graphene *Acc. Chem. Res.* **46** 14–22
[22] Pinilla S, Coelho J, Li K, Liu J and Nicolosi V 2022 Two-dimensional material inks *Nat. Rev. Mater.* **7** 717–35
[23] Citarella A, Amenta A, Passarella D and Micale N 2022 Cyrene: a green solvent for the synthesis of bioactive molecules and functional biomaterials *Int. J. Mol. Sci.* **23** 15960
[24] Hernández-Pagán E, Yazdanshenas A, Boski D J, Bi J, Lacey H R, Piza O J M and Sierra C C S 2024 Cyrene as solvent for metal nanoparticle synthesis *J. Nanopart. Res.* **26** 200
[25] Stini N A, Gkizis P L and Kokotos C G 2022 Cyrene: a bio-based novel and sustainable solvent for organic synthesis *Green Chem.* **24** 6435–49
[26] Milescu R A, McElroy C R, Taylor E J, Williams P M, Phillips R, Farmer T J and Clark J H 2024 Sustainable nanomaterials: the role of cyrene in optimising carbon nanotubes dispersion and filtration efficiency *Front. Chem.* **12** 1498279
[27] Adam J *et al* 2023 The effectiveness of cyrene as a solvent in exfoliating 2D TMDs nanosheets *Int. J. Mol. Sci.* **24** 10450
[28] Poon R and Zhitomirsky I 2020 Application of cyrene as a solvent and dispersing agent for fabrication of Mn3O4-carbon nanotube supercapacitor electrodes *Colloid Interface Sci. Commun.* **34** 100226
[29] Tkachev S, Monteiro M, Santos J, Placidi E, Hassine M B, Marques P, Ferreira P, Alpuim P and Capasso A 2021 Environmentally friendly graphene inks for touch screen sensors *Adv. Funct. Mater.* **31** 2103287
[30] Hernandez Y *et al* 2008 High-yield production of graphene by liquid-phase exfoliation of graphite *Nat. Nanotechnol.* **3** 563–8
[31] Salavagione H J, Sherwood J, De Bruyn M, Budarin V L, Ellis G J, Clark J H and Shuttleworth P S 2017 Identification of high performance solvents for the sustainable processing of graphene *Green Chem.* **19** 2550–60
[32] Pan K, Fan Y, Leng T, Li J, Xin Z, Zhang J, Hao L, Gallop J, Novoselov K S and Hu Z 2018 Sustainable production of highly conductive multilayer graphene ink for wireless connectivity and IoT applications *Nat. Commun.* **9** 1–10
[33] Sherwood J, De Bruyn M, Constantinou A, Moity L, McElroy C R, Farmer T J, Duncan T, Raverty W, Hunt A J and Clark J H 2014 Dihydrolevoglucosenone (cyrene) as a bio-based alternative for dipolar aprotic solvents *Chem. Commun.* **50** 9650–2
[34] Paolucci V, D'Olimpio G, Lozzi L, Mio A M, Ottaviano L, Nardone M, Nicotra G, Le-Cornec P, Cantalini C and Politano A 2020 Sustainable liquid-phase exfoliation of layered materials with nontoxic polarclean solvent *ACS Sustain. Chem. Eng.* **8** 18830–40
[35] Biesinger M C 2022 Accessing the robustness of adventitious carbon for charge referencing (correction) purposes in XPS analysis: insights from a multi-user facility data review *Appl. Surf. Sci.* **597** 153681
[36] Coelho J, Pokle A, Park S H, McEvoy N, Berner N C, Duesberg G S and Nicolosi V 2017 Lithium titanate/carbon nanotubes composites processed by ultrasound irradiation as anodes for lithium ion batteries *Sci. Rep.* **7** 7614
[37] Chavalekvirat P, Hirunpinyopas W, Deshsorn K, Jitapunkul K and Iamprasertkun P 2024 Liquid phase exfoliation of 2D materials and its electrochemical applications in the data-driven future *Precis. Chem.* **2** 300–29
[38] Ng K L *et al* 2023 Direct evidence of the exfoliation efficiency and graphene dispersibility of green solvents toward sustainable graphene production *ACS Sustain. Chem. Eng.* **11** 58–66
[39] Riyajuddin S, Azmi K, Pahuja M, Kumar S, Maruyama T, Bera C and Ghosh K 2021 Super-hydrophilic hierarchical Ni-foam-graphene-carbon nanotubes-Ni2P-CuP2Nano-architecture as efficient electrocatalyst for overall water splitting *ACS Nano* **15** 5586–99
[40] Riyajuddin S, Kumar S, Gaur S P, Sud A, Maruyama T, Ali M E and Ghosh K 2020 Linear piezoresistive strain sensor based on graphene/g-C3N4/PDMS heterostructure *Nanotechnology* **31** 295501
[41] Silva D L *et al* 2020 Raman spectroscopy analysis of number of layers in mass-produced graphene flakes *Carbon N* Y **161** 181–9
[42] Nagyte V *et al* 2020 Raman fingerprints of graphene produced by anodic electrochemical exfoliation *Nano Lett.* **20** 3411–9
[43] Papanai G S, Sharma I and Gupta B K 2020 Probing number of layers and quality assessment of mechanically exfoliated graphene via Raman fingerprint *Mater. Today Commun.* **22** 100795
[44] Datsyuk V, Kalyva M, Papagelis K, Parthenios J, Tasis D, Siokou A, Kallitsis I and Galiotis C 2008 Chemical oxidation of multiwalled carbon nanotubes *Carbon N* Y **46** 833–40
[45] Skaltsas T, Ke X, Bittencourt C and Tagmatarchis N 2013 Ultrasonication induces oxygenated species and defects onto exfoliated graphene *J. Phys. Chem.* C **117** 23272–8
[46] Mendoza-Sánchez B, Rasche B, Nicolosi V and Grant P S 2013 Scaleable ultra-thin and high power density graphene electrochemical capacitor electrodes manufactured by aqueous exfoliation and spray deposition *Carbon N* Y **52** 337–46
[47] Shi X, Wu Z S, Qin J, Zheng S, Wang S, Zhou F, Sun C and Bao X 2017 Graphene-based linear tandem micro-supercapacitors with metal-free current collectors and high-voltage output *Adv. Mater.* **29** 1703034
[48] Zhang C J, Higgins T M, Park S H, O'Brien S E, Long D, Coleman J N and Nicolosi V 2016 Highly flexible and transparent solid-state supercapacitors based on RuO2/PEDOT:PSS conductive ultrathin films *Nano Energy* **28** 495–505
[49] Khasim S, Pasha A, Badi N, Lakshmi M and Mishra Y K 2020 High performance flexible supercapacitors based on secondary doped PEDOT–PSS–graphene nanocomposite films for large area solid state devices *RSC Adv.* **10** 10526–39

[50] Su Z, Jin Y, Wang H, Li Z, Huang L and Wang H 2022 PEDOT:PSS and its composites for flexible supercapacitors *ACS Appl. Energy Mater.* **5** 11915–32
[51] Pimsawat A, Tangtrakarn A, Pimsawat N and Daengsakul S 2019 Effect of substrate surface roughening on the capacitance and cycling stability of Ni(OH)2 nanoarray films *Sci. Rep.* **9** 1–11
[52] Pameté E, Köps L, Kreth F A, Pohlmann S, Varzi A, Brousse T, Balducci A and Presser V 2023 The many deaths of supercapacitors: degradation, aging, and performance fading *Adv. Energy Mater.* **13** 2301008
[53] Jurczakowski R, Hitz C and Lasia A 2004 Impedance of porous Au based electrodes *J. Electroanal. Chem.* **572** 355–66
[54] Bisquert J and Garcia-Belmonte G Fabregat-Santiago F and Compte A 1999 Anomalous transport effects in the impedance of porous film electrodes *Electrochem. Commun.* **1** 429–35
[55] de Levie R 1963 On porous electrodes in electrolyte solutions: i. capacitance effects *Electrochim. Acta* **8** 751–80
[56] Coelho J, Correia R F, Silvestre S, Pinheiro T, Marques A C, Correia M R P, Pinto J V, Fortunato E and Martins R 2023 Paper-based laser-induced graphene for sustainable and flexible microsupercapacitor applications *Mikrochim. Acta* **190** 1–10
[57] Abreu R, Dos Santos Klem M, Pinheiro T, Vaz Pinto J, Alves N, Martins R, Carlos E and Coelho J 2024 Direct laser writing of MnOx decorated laser-induced graphene on paper for sustainable microsupercapacitor fabrication *FlatChem* **46** 100672
[58] Say M G, Brooke R, Edberg J, Grimoldi A, Belaineh D, Engquist I and Berggren M 2020 Spray-coated paper supercapacitors *npj Flex. Electron.* **4** 14
[59] Neff T and Krueger A 2024 A spray coated high performing metal-free onion-like carbon supercapacitor for sustainable energy storage *Electrochem. Commun.* **167** 107798
[60] Miao L, Song Z, Zhu D, Li L, Gan L and Liu M 2020 Recent advances in carbon-based supercapacitors *Mater. Adv.* **1** 945–66
[61] Faruk O and Adak B 2023 Recent advances in PEDOT:PSS integrated graphene and MXene-based composites for electrochemical supercapacitor applications *Synth. Met.* **297** 117384
[62] Cheng B, Wan L, Du C, Ye H, Tian Z and Xie M 2024 Reduced graphene composited N-containing polymer engineered by ball milling as electrode for high-volumetric-performance supercapacitor *J. Energy Storage* **99** 113259
[63] Liu W *et al* 2023 Mechanically flexible reduced graphene oxide/carbon composite films for high-performance quasi-solid-state lithium-ion capacitors *J. Energy Chem.* **80** 68–76